

Enhancement of surface activity in CO oxidation on Pt(110) through spatiotemporal laser actuation

L. Qiao, X. Li,* I. G. Kevrekidis,[†] and C. Punckt

Department of Chemical Engineering, Princeton University, Princeton, NJ 08544 USA

H. H. Rotermund

*Department of Physics and Atmospheric Science,
Dalhousie University Halifax, Nova Scotia, B3H 3J5 Canada*

(Dated: February 2, 2008)

We explore the effect of spatiotemporally varying substrate temperature profiles on the dynamics and resulting reaction rate enhancement for the catalytic oxidation of CO on Pt(110). The catalytic surface is “addressed” by a focused laser beam whose motion is computer-controlled. The averaged reaction rate is observed to undergo a characteristic maximum as a function of the speed of this moving laser spot. Experiments as well as modelling are used to explore and rationalize the existence of such an optimal laser speed.

PACS numbers: 82.40.Ck, 82.40.Np, 05.45.-a

I. INTRODUCTION

A crucial component of chemical engineering process design is to locate optimal operating conditions, which yield optimized productivity, selectivity and flexibility under safety and environmental constraints. Typically one searches for optimal *steady state* conditions, possibly stabilized through feedback loops; yet it is also well-known that non-steady-state operating conditions may lead to better average performance [1]. Examples of such chemical engineering processes include fast pressure swing adsorption [2] and reverse flow reactors [3]. Improvement of the average process performance under non-steady-state conditions (e.g. periodically varying reaction conditions) can sometimes be rationalized through certain resonances between the characteristic operation time scale (e.g. the period of forcing) and the intrinsic time scales of the system [4].

Catalytic reaction systems often exhibit rich nonlinear dynamic behavior, including spatiotemporal patterns such as propagating reacting fronts, pulses, rotating spirals and even chaos [5, 6, 7]. Since the emergence of these spatiotemporal patterns is governed by the system intrinsic time and length scales, catalytic systems may be promising testing fields for optimal non-steady-state operating policies [8]. The development of advanced surface resolving techniques such as PEEM [9, 10], EMSI [11], and RAM [12] has facilitated the observation of catalytic spatiotemporal patterns at the micron scale. Related advances in spatiotemporally addressing catalytic surfaces at the micron scale, in particular through computer-controlled laser beams, have enabled us to spatiotempo-

rally modify local reaction conditions in real time: pulses and fronts, the building blocks of spatiotemporal patterns, can be initiated, erased or guided through appropriate local laser actuation in space and time [13].

In a previous experimental study of modifying the local catalytic surface activity in CO oxidation on Pt(110) through local laser actuation, it was discovered that optimal laser scanning policies exist, maximizing overall reaction (i.e. CO₂ production) rate when the system is close to the excitable regime [14]. The reaction conditions used in those experiments were selected in a way such that the system was initially at a CO-poisoned state (with Pt surface dominated by adsorbed CO which leads to low CO₂ production rate), but could become locally excitable upon local laser heating. The actuation of the laser beam converts the local Pt surface to an excitable state by increasing the local temperature and hence accelerating the desorption of CO. When the laser beam is kept at a fixed position, reacting oxygen pulses are periodically initiated around the laser heating center, and propagate away with significant higher local reaction rate. When the laser beam is scanned at a constant speed, it continuously locally excites the Pt surface [15]. Depending on the intensity of the laser, the spatiotemporal “policy” at which it scans the surface, its scanning speed, and the characteristic times required for the surface to return - after excitation- to the quenched state, different maxima in the overall CO₂ production rate were observed and partially rationalized in Ref. [14].

In order to systematically explore optimal operating conditions we choose a simple laser scanning policy (constant speed “dragging” along a one-dimensional path, [15]) and attempt to establish a quantitative connection between the laser scanning policy and the corresponding overall CO₂ production rate. This is attempted through modelling of the appropriate catalytic reaction-diffusion system with spatiotemporal laser actuation. As a first step, we studied the simple case in which the laser was scanned in a fixed circular pattern at various speeds,

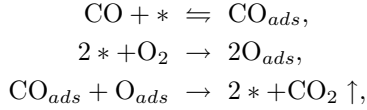
*Present Address: Merck Research Laboratories, West Point, Pennsylvania, PA 19486, USA

[†]Also at the Program in Applied and Computational Mathematics (PACM), Princeton University, Princeton, NJ 08544, USA

through both numerical bifurcation analysis and simulations. By identifying a certain pulse instability associated with the dragging of the laser spot, our computational results could predict the existence of a local maximum in overall CO₂ production rate while varying the laser scanning speed, in agreement with the experiments. The paper is organized as follows. We begin with a brief description of our model of CO oxidation on Pt(110) with local laser dragging. Computational results from numerical bifurcation analysis and transient simulations are then presented and discussed. We also briefly describe the experimental setup and present the experimental results; we conclude with a discussion of the relation between experiments and modeling, and possible extensions of the work.

II. MODELLING

The experimental system of interest is the UHV oxidation of CO on Pt(110); we therefore use the Krischer-Eiswirth-Ertl (KEE) reaction-diffusion model for this reaction [16]. The surface reaction follows a Langmuir-Hinshelwood mechanism:



accompanied by a $1 \times 2 \rightarrow 1 \times 1$ phase transition of the Pt(110) surface due to CO adsorption. The equations for this kinetic model are

$$\dot{u} = k_u s_u p_{\text{CO}} \left[1 - \left(\frac{u}{u_s} \right)^3 \right] - k_1 u - k_2 uv + \nabla \cdot (D_u \nabla u), \quad (1)$$

$$\dot{v} = k_v p_{\text{O}_2} [w s_{v_1} + (1 - w) s_{v_2}] \left(1 - \frac{u}{u_s} - \frac{v}{v_s} \right)^2 - k_2 uv, \quad (2)$$

$$\dot{w} = k_3 (f(u) - w), \quad (3)$$

where u , v and w denote the surface coverage of CO, O, and the surface fraction of the 1×1 phase respectively. The adsorption rate constants for CO and O₂, k_u and k_v respectively, are set to fixed values within the temperature range considered in this paper. The rate constants k_1 , k_2 and k_3 for the desorption, reaction and surface phase transition are temperature dependent through the Arrhenius formula $k_i = k_i^0 \exp(-E_i/kT)$; T is the temperature of the single crystal. We used the parameters for Pt(110) given in Table II of Ref. [16] as follows:

$$u_s = 1, v_s = 0.8, s_u = 1, s_{v_1} = 0.6, s_{v_2} = 0.4,$$

$$k_u = 3.135 \times 10^5 \text{ s}^{-1} \text{ mbar}^{-1},$$

$$k_v = 5.858 \times 10^5 \text{ s}^{-1} \text{ mbar}^{-1},$$

$$k_i = k_i^0 \exp(-E_i/kT), i = 1, 2, \text{ and } 3,$$

$$k_1^0 = 2 \times 10^{16} \text{ s}^{-1}, E_1 = 38 \text{ kcal/mol},$$

$$k_2^0 = 3 \times 10^6 \text{ s}^{-1}, E_2 = 10 \text{ kcal/mol},$$

$$k_3^0 = 10^2 \text{ s}^{-1}, E_3 = 7 \text{ kcal/mol}.$$

We adopted the diffusion coefficients reported in Ref. [17]:

$$D_u = D_u^0 \exp(-E_u/kT)$$

where, in the $[1\bar{1}0]$ direction, $D_u^0 = 5 \times 10^{-3} \text{ cm}^2/\text{s}$, $E_u = 10 \text{ kcal/mol}$ and in the $[001]$ direction $D_u^0 = 7 \times 10^{-4} \text{ cm}^2/\text{s}$, $E_u = 8.9 \text{ kcal/mol}$. The function $f(u)$ has been fitted to experimental data to give the rate of surface phase transition as a function of u , the coverage of CO, as follows:

$$f(u) = \begin{cases} 0 & \text{for } u \leq 0.2, \\ \frac{u^3 - 1.05u^2 + 0.3u - 0.026}{-0.0135} & \text{for } 0.2 < u < 0.5, \\ 1 & \text{for } u \geq 0.5. \end{cases}$$

In Eqs. (1)-(3) the temperature field is assumed to be homogeneous across the catalytic surface and prescribed by a single parameter T . When a laser beam is scanned across the sample surface, the local temperature of the catalytic surface around the laser spot is temporarily increased, leading to spatiotemporal heterogeneity in the surface temperature field. In order to model such a spatiotemporal heterogeneous temperature field, we make the following two simplifications [18, 19]: a) the heat generated by the CO oxidation reaction on the Pt(110) surface ($\sim 1 \text{ mW}/\text{cm}^2$) is neglected compared to the power of the laser beam ($\sim 1 \text{ W}$ for a crystal surface of $75 \mu\text{m}$ in diameter (size of the laser spot)); b) we consider that the local temperature profile inhomogeneity is established (and then vanishes) instantly as the laser beam is applied (and then removed). This is because the time scale associated with the local temperature change ($\sim 10^{-3}$ second, estimated from W^2/α , where W is the diameter of the laser spot ($75 \mu\text{m}$) and α is the thermal diffusivity of Pt ($\sim 10^{-1} \text{ cm}^2/\text{s}$)) is much smaller than the time scales of local adsorbate coverage change ($\sim 10^{-1}$ second and ~ 1 second, estimated from CO desorption with $1/k_1$ and CO diffusion with W^2/D_u). Based on these two simplifications, the spatiotemporal change in the temperature field induced by a moving laser beam can be modelled as a temperature “bump” with fixed shape co-travelling with the laser spot.

In the experiments, the laser beam is moved in a circular path on the sample surface at constant speed. Because the typical diameter of the circular path ($\sim 860 \mu\text{m}$) is significantly larger than the size of the laser spot ($\sim 75 \mu\text{m}$ in diameter), it is informative to model the laser scanning in one dimension with periodic boundary conditions. A computational frame co-travelling with the laser spot is introduced. Based on the KEE model and the discussion above, we have the following equations for CO oxidation in a one-dimensional periodic domain with laser scanning in a co-moving frame:

$$u_t = k_u s_u p_{\text{CO}} \left[1 - \left(\frac{u}{u_s} \right)^3 \right] - k_1 u - k_2 uv + (D_u u_z)_z + c u_z, \quad (4)$$

$$v_t = k_v p_{\text{O}_2} [w s_{v_1} + (1-w) s_{v_2}] \left(1 - \frac{u}{u_s} - \frac{v}{v_s} \right)^2 - k_2 uv + c v_z, \quad (5)$$

$$w_t = k_3 (f(u) - w) + c w_z, \quad (6)$$

where c is the speed of the co-moving frame (equal to the laser moving speed); z is the spatial coordinate in the co-moving frame with $z \equiv x - ct$; and the remaining symbols are the same as in Eqs. (1)-(3), except k_1 , k_2 and k_3 , which are now spatially dependent because of the nonuniform temperature field $T(z)$ due to local laser heating. In the computations the local $T(z)$ heterogeneity due to the laser spot is approximated by a Gaussian profile.

III. COMPUTATIONAL RESULTS

For simplicity, we first consider the case where the diffusion of CO in our one-dimensional domain is isotropic (i.e. constant D_u). With this assumption, the coverage profile of the adsorbates in a *static* observation frame eventually becomes periodic in both space and time, when a laser beam is periodically scanned across the domain at a fixed speed c . This oscillatory solution (in the static observing frame) corresponds to a *steady state* solution in the co-moving frame (i.e. of Eqs. (4)-(6)). A Newton-Raphson iteration combined with pseudoarclength continuation is used on Eqs. (4)-(6) to compute and continue the corresponding steady coverage profiles as the laser dragging speed, c , is varied (that is also the speed of the resulting dragged pulse). The CO_2 production rate is then averaged over the entire domain for each steady coverage profile and plotted against c , as shown in Fig. 1. The reported enhancement is in comparison to the reaction rate at the quenched state (without laser illumination). Note that the steady profiles of adsorbate coverages computed through pseudoarclength continuation may be unstable (the dashed line in Fig. 1), which can lead to an estimate of the average CO_2 production

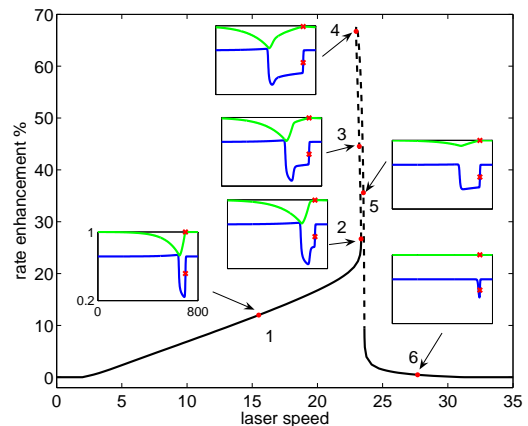


FIG. 1: (Color online) Enhancement in the CO_2 production rate as a function of the laser scanning speed for isotropic CO diffusion. The steady coverage profile is computed in a frame co-travelling with the laser spot. Stable (unstable) steady coverage profiles are marked in solid (dashed) lines. Representative coverage profiles are shown in the insets, where the blue and green curves represent the coverage of CO and the fraction of the 1×1 phase respectively. The coverage of CO and the fraction of the 1×1 phase at the center of the laser spot are marked by red crosses. Parameters used: domain length $L = 800$, space discretization $\Delta x = 0.25$ with periodic boundary conditions. The local temperature field around the laser spot is approximated by a Gaussian profile ($\sigma = 2$), with a maximum temperature increase $\Delta T = 5\text{K}$ at the laser spot center $x = 700$. Reaction conditions: $T = 541\text{K}$, $p_{\text{CO}} = 4.68 \times 10^{-5} \text{ mbar}$, $p_{\text{O}_2} = 1.33 \times 10^{-4} \text{ mbar}$. The unit dimensionless time and length correspond to real values of 1 s and $\sim 5.6 \mu\text{m}$ respectively. The unit dimensionless speed thus corresponds to a real speed of $\sim 5.6 \mu\text{m/s}$.

rate very different from direct simulations (through time integration) at fixed c . We will discuss this in detail at the end of this section.

In Fig. 1, when the laser dragging speed is increased from zero to approximately 23 (at point 2), the steady profiles of the adsorbate coverage retain a pulse-like appearance. Such pulse-like profiles gradually start to “lag behind” the laser spot, as the laser dragging speed increases, which leads to a monotonic increase in the overall CO_2 production rate to 20% compared to the quenched state. Following the solution branch from point 2 to point 4 in the Figure, the pulse-like structure gradually dissolves and a “plateau” in the CO coverage profile starts to develop between the center of the laser spot and the lagging pulse-like structure. The “pulse” now appears to consist of two distinct fronts - a leading and a trailing one. After point 4, the plateau also starts to shrink and finally disappears around $c = 24$. Such a process occurs in a very narrow range of c (approximately between 23 to 24) and causes a very sharp increase in the overall CO_2 production rate enhancement (up to 70%) followed by an immediate sharp decrease (down to approximately 5%), which is apparently associated with the development and

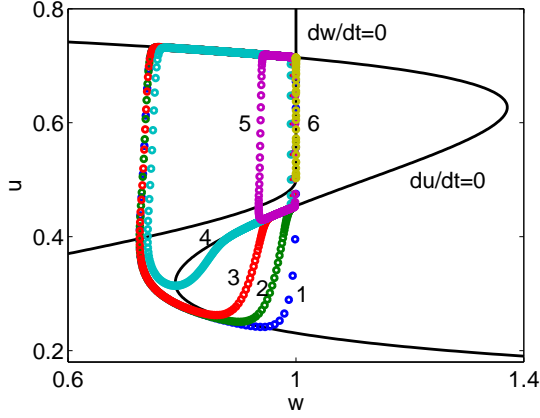


FIG. 2: (Color online) Phase portraits (circles) for steady coverage profiles at different c values (points 1 to 6 as in Fig. 1), see text.

disappearance of a wide plateau in the CO coverage profile. When the laser scanning speed is increased above 24, the rate enhancement quickly drops to zero.

The emergence of the pulse-like structure and the plateau in CO coverage profile is thus seen to be intimately related to the rate enhancement. In order to better understand the nature of this relation, we explore the connection between the steady spatial coverage profiles and the dynamics of the KEE ODE model, as shown in Fig. 2. It has been argued [20] that, since the oxygen adsorption is much faster than CO desorption, the temporal variation of oxygen coverage can be adiabatically eliminated for simplification, leading to a reduced two-variable model (for u and w). The corresponding nullclines of this two-dimensional model are plotted in Fig. 2 (solid lines). Representative dragged pulse coverage profiles in the co-moving frame (e.g. points 1 to 6 in Fig. 1) correspond to limit cycles (periodic trajectories) of the ODE system (in z) obtained by setting the left side of Eqs. (4)-(6) to zero. These u and w profiles are superposed on the simplified two-equation model nullclines in Fig. 2 (circles).

The trajectories corresponding to points 1 to 3 “reach down” to the lower branch of the $du/dt = 0$ nullcline, confirming the pulse-like nature of the pattern that results from laser-dragging. The CO plateau structure, clearly seen in the spatial coverage profiles corresponding to points 3 to 5, are associated with the profile remaining close to the middle branch of the $du/dt = 0$ nullcline. This “overlap” with the middle branch shrinks as the laser scanning speed c is increased. In dynamical systems terminology, this plateay structure is thus associated with a “canard” [21]. For point 6, the trajectory does not attain the middle branch of the $du/dt = 0$ nullcline; it aligns with the $dw/dt = 0$ nullcline.

Based on the discussion above, the relationship between the enhancement in CO_2 production rate and the laser dragging speed c , as shown in Fig. 1, can be partially rationalized as follows: When c is increased from

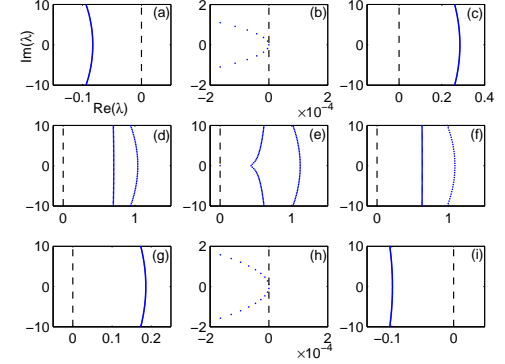
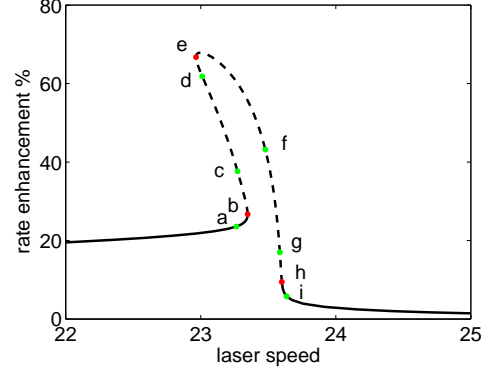


FIG. 3: (Color online) A blow-up picture of the unstable solution branch (dashed line) in Fig. 1. Bifurcation points are marked by red dots. Following the solution branch from left to right, representative eigenvalue spectra (marked by dots) corresponding to the labelled points are plotted in the insets below.

zero up to values in the neighborhood of point 2 (~ 23.3), the laser spot locally excites the catalytic surface, creates and “drags along” a reacting pulse (e.g. point 1). Such a pulse remains attached to the laser spot; it starts becoming more spatially extended as c is increased, leading to a monotonic increase in production rate (appreciable adsorbed CO and oxygen coexisting over longer spatial extents). When c becomes too fast for the laser actuation to excite the local catalytic surface, the brief temperature increase effected by the passage of the laser spot only leads to a small local variation in the coverage profile (e.g. point 6). For values of c between the two limiting cases above (e.g. between points 2 and 5 in Fig. 1), the steady coverage profiles computed from pseudoarclength continuation become unstable. In this case, direct simulations must be used to find what the stable long-term behavior is, and thus establish a connection between c and the corresponding rate enhancement (see below).

A blow-up of the unstable solution branch in Fig. 1 is shown in Fig. 3 along with the corresponding eigenvalue spectra of the system linearization in the neighborhood of the bifurcation points. These linearization spectra have

been computed in a finite but long domain with periodic boundary conditions; computed eigenvalues are marked by dots, and the density of these dots is suggestive of continuous spectrum components for the infinite domain problem.

As we move from point *a* to point *c*, a “parabola” of eigenvalues crosses the imaginary axis from left to right. For our large but finite periodic problem, the leading eigenvalue (the eigenvalue(s) with largest real part on this parabola) is a single real one (as in inset (b)). The initiation of the crossing of such an “eigenvalue parabola” corresponds to a Saddle-Node (SN) bifurcation followed by a large number of subsequent Hopf bifurcations. As *c* varies from point *c* to point *d*, the leading spectrum component appears to split in two. At point *e* a single real eigenvalue (whose path started close to the parabolic spectrum component farthest to the left from the imaginary axis) crosses the imaginary axis, corresponding to another SN bifurcation. From points *f* to *g*, the split spectrum components appear merge again into a single component, which then crosses the imaginary axis from right to left (see point *h*). The leading eigenvalues of this new parabolic spectrum component (the last ones to cross to stability) are now a conjugate pair (in contrast to point *e*). The crossing of such a component of the spectrum appears in our finite domain case as (from point *g* to point *i*) as a chain of Hopf bifurcations. Continuous eigenvalue spectrum crossing has been shown to be associated with the emergence of “chemical turbulence” for CO oxidation in an excitable medium [22].

For values of *c* for which the dragged pulse solutions are unstable, direct simulation is used to establish the nature of the observed dynamics (and to find the corresponding average reaction rate). Phase diagrams of the long-term dynamics for such simulations appear quasiperiodic or mildly chaotic, and do not repeat exactly (as shown in Fig. 4). For sufficiently large domains (as was the case here), the approximate period of the oscillations is not affected by the domain length. In this regime, as *c* is increased, the system spends less time on average in states with a long, reacting pulse-like tail, which leads to a decrease in the overall (space-time averaged) CO₂ production rate. This is consistent with the (spatiotemporally) averaged reaction rate monotonically decreasing as *c* varies from points *e* through *h* in Fig. 3.

Anisotropic CO Diffusion. To incorporate the effect of diffusion anisotropy for the adsorbed CO on Pt(110), we approximate the anisotropic diffusion coefficient with a spatially periodic function, $D_u \equiv (D_{uf} + D_{us})/2 + (D_{uf} - D_{us})/2 \times \sin(4\pi x/L)$, where D_{uf} and D_{us} correspond to the coefficients of CO diffusion on Pt(110) in the fast ([1 $\bar{1}$ 0]) and in the slow ([001]) directions respectively. The interaction between laser scanning and strong anisotropic CO diffusion is illustrated in Fig. 5, which shows that the reacting tails only exist in regions where the local CO diffusion is slow. To visually enhance this phenomenon, and also to show how different the instantaneous pulse profiles can be as the laser

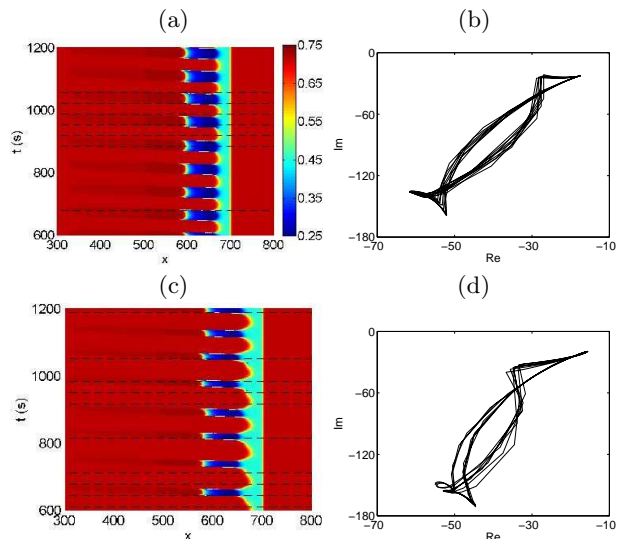


FIG. 4: (Color online) Space-time plots and phase portraits of CO coverage dynamics for different laser scanning speeds in the unstable regime. (a) and (c), space-time plots of CO coverage for $c = 23.5$ and 23.6 respectively. (b) and (d), the corresponding phase portraits of the first fast Fourier transform component of the CO spatial coverage profile. When *c* is increased the system spends less time on average at a state with a long reacting tail; thus the overall CO₂ production rate is less in (c) as compared with (a). The time interval between dashed lines in (a) and (c) corresponds to L/c , that is, one “rotation” of the laser beam along the periodic domain.

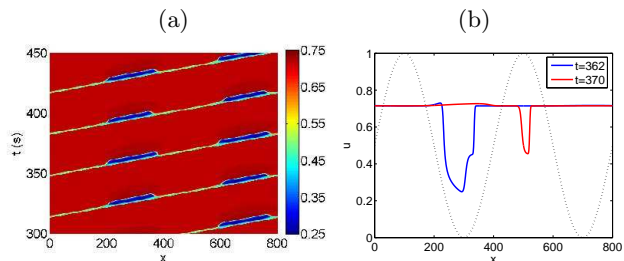


FIG. 5: (Color online) Laser scanning in the presence of strong anisotropic CO diffusion. (a) space-time plot of CO coverage in a frame co-traveling with the laser spot; (b) representative instantaneous snapshots of the CO coverage profile. The anisotropic diffusion of CO is approximated by a periodic diffusion coefficient with a period of $L/2$ (dotted line in (b)), $D_u \equiv (D_{uf} + D_{us})/2 + (D_{uf} - D_{us})/2 \times \sin(4\pi x/L)$, where D_{uf} and D_{us} correspond to the diffusion coefficient values along the fast and slow directions on Pt(110) respectively. $D_{uf}/D_{us} = 3$, $c = 23.3$.

rotates on the surface Fig. 5 employs diffusion coefficient values six times as large as the ones reported in [17] (but with the correct anisotropy ratio). Resetting D_{uf} and D_{us} to their experimentally reported values [17], time integrations of Eqs. (4) to (6) show periodic or apparently quasiperiodic transient behavior (Fig. 7). In both cases we average the reaction rate over both the domain length and a long enough time interval to compute the corre-

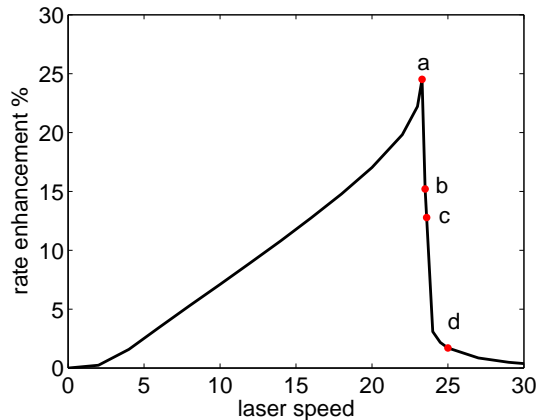


FIG. 6: Averaged rate enhancement in CO_2 production as a function of laser scanning speed for anisotropic CO diffusion. For a fixed laser scanning speed, the CO_2 production rate is computed based on the spatiotemporal coverage profile, averaged over the entire domain and a sufficiently long time interval. D_{uf} and D_{us} are estimated from experimental data [17]; $D_{uf}/D_{us} = 3$.

sponding average enhancement in CO_2 production rate shown in Fig. 6. When c is varied between 0 and approximately 23, the dynamics in the co-moving frame converge to a stable oscillatory state with a period of $L/(2c)$. During the oscillations, the length of the reacting tail only slightly varies as the local CO diffusion coefficient modulates (not shown). Similar behavior has been observed for larger c (i.e. > 24), where the width of local coverage profile around the laser spot slightly modulates. Compared with the isotropic case, the averaged rate enhancement shows the same qualitative behavior for the two limiting cases: for smaller c the rate enhancement gradually increases as c is increased; for large c the rate enhancement suddenly decreases as c is increased. When c is in the intermediate range $23 \sim 24$ (associated with instability in the isotropic case), the system can show distinct quasiperiodic transient behavior: for c close to the lower boundary of this interval the system exhibits oscillations similar to the corresponding isotropic case (Fig. 7(b)); for c close to the upper boundary, “skipping” oscillations can be observed, as shown in Fig. 7(c). By comparing the position of reacting tails in Fig. 7(c) with the corresponding spatial profile of D_u , we find that the reacting tails occur only along the slow diffusion directions (when the local D_u is small). This suggests that the local periodic change in CO diffusion coefficient as the laser spot moves along a ring can have a strong impact on the local dynamics; it can, for example temporarily eliminate a reacting tail and then reestablish it (see the small time gap in Fig. 7(c) when the reacting tail disappears). As in the isotropic case, the averaged rate enhancement in this range of c monotonically decreases as c is increased.

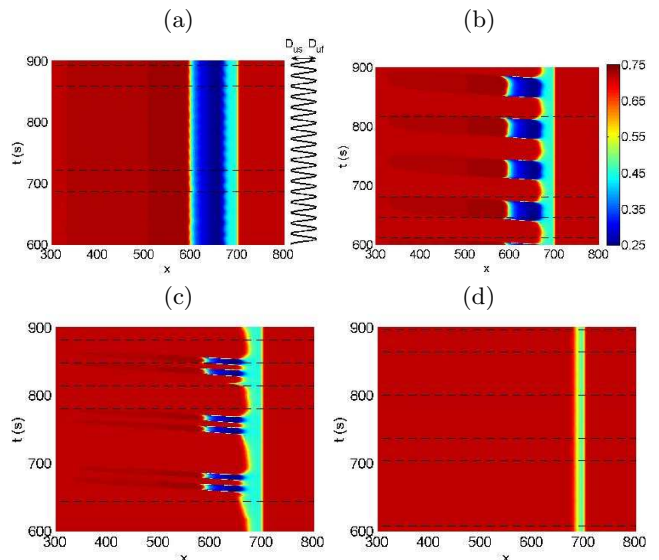


FIG. 7: (Color online) Phase portraits for anisotropic CO diffusion at different laser scanning speeds. The local CO diffusion coefficient at $x = 700$ is plotted on the right of plot (a). (a) $c = 23.3$, (b) $c = 23.5$, (c) $c = 23.6$, (d) $c = 25$.

IV. EXPERIMENTS

The simplest motion of a temperature heterogeneity on the platinum surface would be a linear one, on an infinitely extended catalyst. This cannot be realized in the experiment. The easiest consistent approach is to use a protocol where the laser spot moves on a circle with large circumference. This is experimentally feasible and makes a comparison with theory possible. Circular movement was tentatively explored in a previous study [14]; however, the resulting surface dynamics and changes in reaction rate were not analyzed in detail. Here, we show new experimental results, focussing on reaction enhancement and the influence of the laser spot on the reaction patterns; we also compare to the theoretical results presented in the first part of the paper.

Experiments are performed using a Pt(110) single crystal with 10 mm diameter located in an ultra high vacuum (UHV) chamber. For accurate control of the reaction parameters (temperature, CO and oxygen partial pressures), the chamber is equipped with a computer controlled gas dosing system, that allows for adjusting the partial pressures of carbon monoxide and oxygen. The platinum sample is heated from the back with a halogen lamp. For sample preparation and characterization, the chamber is equipped with Ar-ion sputtering and Low-Energy Electron Diffraction (LEED). A tube (~ 38 mm in diameter) with a cone-like ending (~ 4 mm in diameter) is placed about 2 mm away from the sample surface. It connects the reaction chamber with a differentially pumped Quadrupole Mass Spectrometer (QMS) used for analysis of the reaction products. This way, a large fraction of

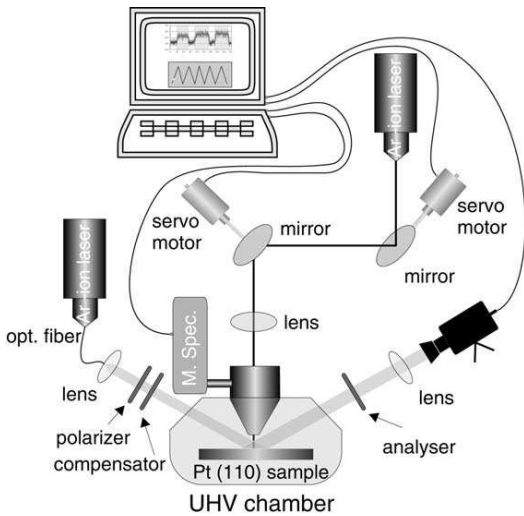


FIG. 8: Schematic view of the experimental setup, not to scale. See the text for details. Reproduced from [14].

the carbon dioxide produced during the reaction can be detected, providing an estimate of the overall surface reaction rate. The carbon monoxide signal detected by the QMS was stored on a computer.

Concentration patterns of CO and oxygen on the sample surface are imaged at a rate of 25 images per second using Ellipsomicroscopy for Surface Imaging (EMSI) [23]. They are recorded with a video CCD camera. The background of the video signal is subtracted and the signal is contrast-enhanced in real time using a downstream Argus 20 image processing unit from Hamamatsu and stored on a video recorder. The surface reaction can be locally manipulated by a Argon ion laser beam which is focussed onto the platinum crystal. The spot size of the laser is approximately $75\ \mu\text{m}$ in diameter. Two computer-controlled mirrors allow for controlled motion of the laser spot on the sample surface. Special motion protocols (like linear or circular trajectories of the laser spot) can be programmed using LabView. The partial pressures of oxygen and CO are also controlled through this software. The experimental setup is sketched in Fig. 8.

At the beginning of each experiment, the laser beam is focussed to a fixed position on the sample surface for several minutes, until the temperature of the crystal equilibrates. This is necessary because the laser spot not only produces a strongly located temperature increase but additionally slightly increases the mean crystal temperature (by a few K). The laser beam is then scanned across the sample surface with a constant speed for 40 seconds, following a fixed circular path with a circumference of approximately 2.7 mm. This is illustrated in Fig. 9. The scanning of the laser beam is stopped for a minute every time before a different scanning speed for the laser beam is applied; at each speed several measurements are performed and their results in terms of reaction rate increase are averaged.

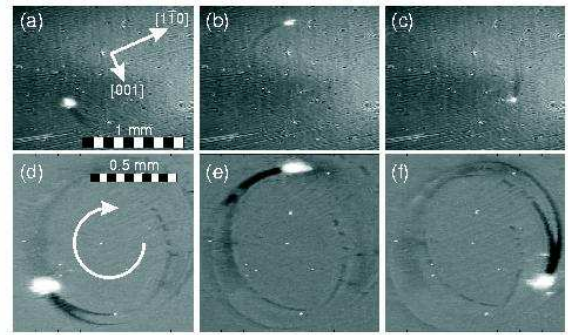


FIG. 9: Circular motion of the laser spot across the platinum catalyst. (a)-(c) raw data, (d)-(f) images after additional background subtraction, contrast enhancement and cropping. The time difference between the snapshots is 0.96 s. The crystal orientation is indicated in (a). Diffusion along the $[1\bar{1}0]$ axis is faster (by an estimated factor of 2-3) than in the $[001]$ direction. The laser spot is visible as a bright white area in the images. Due to the laser motion, a “tail” develops behind the spot. The reaction parameters are $P_{\text{Laser}}=640\ \text{mW}$, $p_{\text{O}_2}=3.00 \times 10^{-4}\ \text{mbar}$, $p_{\text{CO}}=8.43 \times 10^{-5}\ \text{mbar}$, and $T = 513\ \text{K}$.

In EMSI images, dark surface area is associated with more reactive, predominantly oxygen covered surface. When the laser spot moves, a dark tail can be observed: the laser spot removes some adsorbed CO in its path. Since CO poisons the catalytic surface, its removal increases the catalytic activity. In addition to the one-dimensional theoretical observations in the first part of this article, we see here the full two-dimensional structure of the laser induced reactive surface area. At a certain distance from the laser spot, the tail divides, and a “swallowtail” composed of two narrow “tongues” can be seen. Figure 10(a) shows the CO_2 signal measured by the QMS. During the periods of laser spot motion (shaded regions) the CO_2 signal is increased. The delay between stopping the laser spot motion and associated decrease of the CO_2 production rate is due to the slow time scale of the differential pumping of the QMS.

We measure the increase of the carbon dioxide signal as a function of the laser spot velocity. The results are shown in Fig. 10(b). We observe that the average reaction rate increases for velocity values up to about 2.8 mm/s. For higher velocities, the enhancement falls precipitously until the laser spot moves so fast that no enhancement can be measured. When all other reaction parameters are kept fixed, there exists a certain velocity of the laser spot at which the enhancement is at its maximum. We call this velocity value the “optimal velocity”. The experimental curve agrees qualitatively with theory: A slow increase of the reaction rate is followed by a fast decrease after the optimal velocity has been exceeded. This has been observed in our computations both for isotropic and for anisotropic diffusion coefficients; in the case of anisotropic diffusion the dragged pulse profile varies along the laser path because the diffusion coeffi-

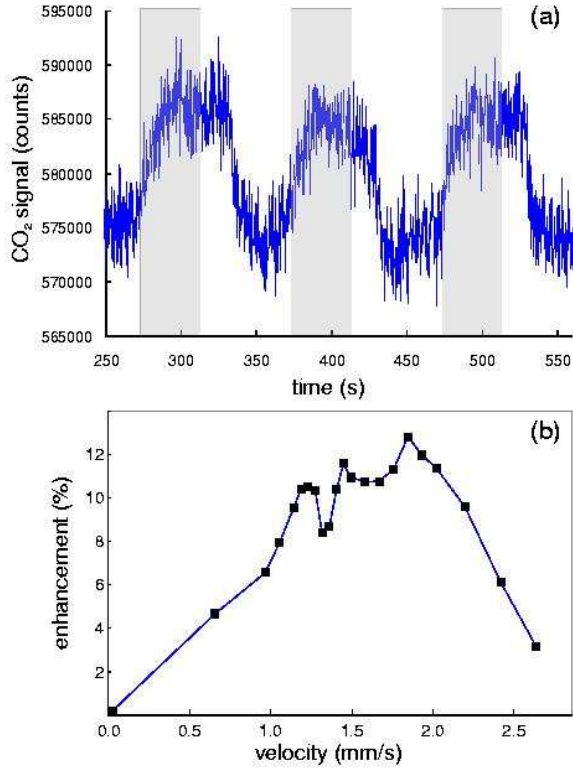


FIG. 10: Enhancement of CO₂ production. (a) QMS signal; the laser spot is only moving during the shaded time intervals with a velocity of 0.91 mm/s. (b) Average enhancement for different velocities of the laser spot. The reaction parameters are $P_{\text{Laser}}=640$ mW, $p_{\text{O}_2}=3.00 \times 10^{-4}$ mbar, $p_{\text{CO}}=8.60 \times 10^{-5}$ mbar, and $T = 512.5$ K.

cient also varies. The variation in the length of the pulse tail in the three snapshots of Fig. 9 is the result of the varying orientation of laser motion with respect to the crystal axes (and the associated CO diffusion coefficient variation).

Figure 11 shows the results of experiments at different reaction parameters, normalized with respect to the optimal velocity of each experiment. The qualitative behavior of the reaction enhancement appears similar in all cases shown. The experimental curves exhibit a clear maximum in the overall rate enhancement as the laser scanning speed is varied, in agreement with the computational results shown above. It is interesting to observe certain secondary reaction extrema “on the way” to the overall maximum as the laser spot velocity increases, e.g. at $v = 1.35$ mm/s in Fig. 10(b). These were not observed in our one-dimensional modeling, and they most probably should be attributed to the two-dimensional nature of the system.

As the laser moves on the catalytic surface, it locally shifts the system into an excitable state. This results in the development of a reactive “tail” behind the laser spot. The length and the width of this tail vary with the spot velocity as clearly seen in Fig. 12. Qualitatively, the variation of the average tail length with the laser

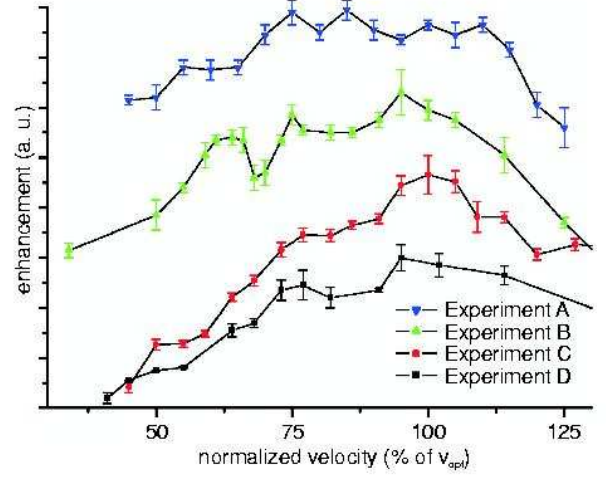


FIG. 11: Reaction rate enhancement at different experimental conditions: Each enhancement curves is normalized with respect to its optimum velocity and arbitrarily shifted with respect to the y axis for better comparison. The reaction conditions were $P_{\text{Laser}}=640$ mW, $p_{\text{O}_2}=3.00 \times 10^{-4}$ mbar, $p_{\text{CO}}=8.60 \times 10^{-5}$ mbar, and $T=512.5$ K for experiments A and B, and $p_{\text{CO}}=8.43 \times 10^{-5}$ mbar, and $T=513$ K for experiments C and D.

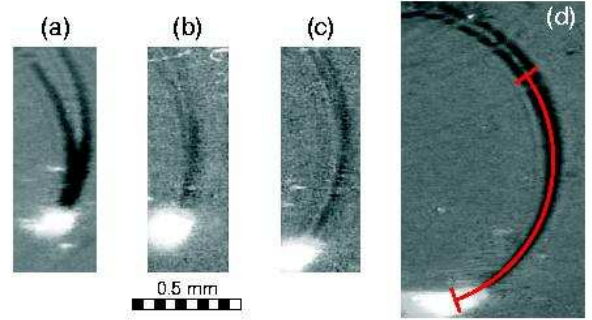


FIG. 12: Length of the dark reactive tail at different velocities. (a) $v=0.94$ mm/s, $l=0.23$ mm, (b) $v=1.2$ mm/s, $l=0.38$ mm, (c) $v=1.8$ mm/s, $l=0.53$ mm, (d) $v=2.6$ mm/s, $l=0.79$ mm, parameters like in Fig. 9.

dragging speed mimicks the variation of the reaction rate enhancement both in modeling and in experiments: the tail initially becomes longer and then precipitously disappears as the speed is increased. However, due to the development of two “tongues” in the back of the tail, a clear definition of the tail length in the experiment is somewhat difficult. We (rather arbitrarily) chose the distance between the laser spot and the point where the tail visibly splits as a measure of the tail length. With increasing laser speed the tail becomes longer and narrower. In Fig. 12 (d) the length of the tail has increased further, yet the reaction enhancement is almost negligible. This appears counterintuitive, since in the theoretical part of this article we saw a clear correlation between tail length and reaction rate enhancement. However, the

one-dimensional modelling ignores the width (and overall two-dimensional structure) of the tail; this makes direct comparison between the two-dimensional experiment and the one-dimensional theory difficult. We expect to report on a more quantitative comparison, based on full two-dimensional simulations, in a future publication. For very high laser speeds in the experiment - as well as in the 1D model- the reactive tail completely vanishes, since the thermal energy deposited per time and surface area in the catalytic surface no longer provides a sufficient local temperature increase to excite the system.

V. SUMMARY AND CONCLUSIONS

Following our initial experimental study [14] on improving catalytic surface activity through time-dependent operating policies, we performed here a systematic exploration of the effect laser spot motion on the average reaction rate of CO oxidation on a Pt(110) surface. Quantitative relations between overall rate enhancement and the laser scanning speed, for both isotropic and anisotropic CO diffusion, have been obtained through numerical bifurcation analysis and direct simulations. A characteristic local maximum in the rate enhancement (gradual increase followed by precipitous drop) has been observed in both cases. The local maximum for isotropic CO diffusion was associated with the development of a pulse instability caused by laser dragging and apparently involving the dragged pulse continu-

ous spectrum. When anisotropic CO diffusion is included in the model, and for a wide range of laser scanning speeds, the system exhibits comparable *averaged* rate enhancement response; yet the anisotropy has a significant qualitative effect on the detailed dynamics (including quasiperiodicity and even mild spatiotemporal chaos). The computational results are supported by experimental observations showing a qualitatively comparable increase of averaged reaction rate with laser scanning velocity. Optimal velocities were obtained experimentally for a range of different reaction conditions. Experimental observations revealed an interesting two-dimensional structure of the dragged pulse “reactive tail”; this clearly suggests that full two-dimensional modeling, taking into account diffusion transverse to the pulse motion, is required for a more quantitative comparison of theory with experiments. We are currently working towards such a fully two-dimensional model study. The laser motion explored in this paper was, in some sense, the simplest spatiotemporal one: effectively one-dimensional with constant speed. Spatiotemporally more complex motions, such as those presented in [14], possibly also containing a stochastic component [24], should provide a rich field of study.

Acknowledgements This work was partially supported by the National Science Foundation and by a Guggenheim Fellowship (I.G.K.). The experiments were performed while two of the authors (C.P., H.-H.R.) were at the Fritz Haber Institute of the Max Planck Society (Physical Chemistry) in Berlin.

-
- [1] J. E. Bailey, Chem. Eng. Comm. **1**, 111 (1973).
 - [2] D. M. Ruthven, S. Farooq, and K. S. Knaebel, *Pressure Swing Adsorption* (Wiley, New York, 1993).
 - [3] Y. S. Matros and G. A. Bunimovich, Catal. Rev. Sci. Eng. **38**, 1 (1996).
 - [4] I. G. Kevrekidis, L. D. Schmidt, and R. Aris, Chem. Eng. Sci. **41**, 1263 (1986).
 - [5] M. C. Cross and P. C. Hohenberg, Rev. Mod. Phys. **65**, 851 (1993).
 - [6] R. Imbihl, Catalysis Today **105**, 206 (2005).
 - [7] R. Imbihl and G. Ertl, Chem. Rev. **95**, 697 (1995).
 - [8] E. Machado, G. M. Buendia, P. A. Rikvold, and R. M. Ziff, Phys. Rev. E **71**, 016120 (2005).
 - [9] H. H. Rotermund, W. Engel, M. Kordesch, and G. Ertl, Nature (London) **343**, 355 (1990).
 - [10] W. Engel, M. E. Kordesch, H. H. Rotermund, S. Kubala, and A. von Oertzen, Ultramicroscopy **36**, 148 (1991).
 - [11] H. H. Rotermund, G. Haas, R. U. Franz, R. M. Tromp, and G. Ertl, Science **270**, 608 (1995).
 - [12] C. Punckt, F. S. Merkt, and H. H. Rotermund, New J. Phys. **9**, 213 (2007).
 - [13] J. Wolff, A. G. Papathanasiou, I. G. Kevrekidis, H. H. Rotermund, and G. Ertl, Science **294**, 134 (2001).
 - [14] A. G. Papathanasiou, J. Wolff, I. G. Kevrekidis, H. H. Rotermund, and G. Ertl, Chem. Phys. Lett. **358**, 407 (2002).
 - [15] J. Wolff, A. G. Papathanasiou, H. H. Rotermund, G. Ertl, X. Li, and I. G. Kevrekidis, Phys. Rev. Lett. **90**, 018302 (2003).
 - [16] K. Krischer, M. Eiswirth, and G. Ertl, J. Chem. Phys. **96**, 9161 (1992).
 - [17] A. von Oertzen, H. H. Rotermund, and S. Nettesheim, Surface Science **311**, 322 (1994).
 - [18] J. Cisternas, P. Holmes, I. G. Kevrekidis, and X. Li, J. Chem. Phys. **118**, 1 (2003).
 - [19] J. Cisternas, P. Holmes, and I. G. Kevrekidis, Physica D **177**, 71 (2003).
 - [20] M. Baer, N. Gottschalk, M. Eiswirth, and G. Ertl, J. Chem. Phys. **100**, 1202 (1994).
 - [21] J. Moehlis, J. Nonlinear Sci. **12**, 319 (2002).
 - [22] M. G. Zimmermann, S. O. Firlé, M. A. Natiello, M. Hildebrand, M. Eiswirth, M. Baer, A. K. Bangia, and I. G. Kevrekidis, Physica D **110**, 92 (1997).
 - [23] H. H. Rotermund, Surf. Sci. **386**, 10 (1997).
 - [24] J. Wolff, A. G. Papathanasiou, H. H. Rotermund, G. Ertl, M. A. Katsoulakis, X. Li, and I. G. Kevrekidis, Phys. Rev. Lett. **90**, 148301 (2003).